the original bar's visibility would be sufficiently reduced for at least one of these delays[25] (Fig. 4). Although the mask was effective, it produced only a slight shift in the target line's colour towards red (Fig. 4), so failing to support the persistence explanation.

Further experiments will reveal the neural basis of this colour phenomenon, which cannot have a retinal origin as the primate retina is unable to distinguish the direction of movement of a target[26]. The effect is probably a by-product of motion extrapolation, which could be accomplished by cortical neurons that demonstrate 'predictive remapping'. For these neurons, the response latency for a target entering the cell's receptive field from some other location is lower than the latency for a target with an abrupt onset in that cell's receptive field[27]. At a given instant, two sets of active cells of this type, one stimulated by a moving object and the other by a retinally superimposed flash, will thus code non-overlapping retinotopic locations. Given the reported interaction between colour and motion, I suggest that some cells that demonstrate predictive remapping are also stimulated by colour input. Finally, my findings not only support the Young–Helmholtz–Maxwell view of colour vision, but also suggest that retinally overlaid red and green signals yield the perception of yellow if, and only if, these signals originate from the same retinotopic locations in the cortex. □

Methods

A d.c. motor connected to a speed controller revolved a green bar ($1.59° \times 0.20°$) anti-clockwise on a circular path (diameter, 7.63°) at 30 r.p.m. (instantaneous speed, $11.46° s^{-1}$). Two horizontal lines (length, 1.27°), separated by 0.91°, were flashed simultaneously for 2 ms at 0.5 hertz. A mirror-type beam-splitter was used to present the flashed lines in the optical plane of the bar. The flash was synchronized with the bar so that the target line was superimposed on the bar. Observers used a chin rest to view the display binocularly through natural pupils. Ambient room lights were turned on about once every 10 s for a comparable period in order to maintain the observer's light adaptation level and pupil size.

Brief-exposure condition. The bar was visible only through a $1.59° \times 0.20°$ window. The duration of visibility was ~17.45 ms. The colour of the comparison line was held constant at green–yellow. On ten trials the experimenter adjusted the bar's intensity until the observer indicated that the target line matched the comparison line in colour. The average of the bar intensities for each observer was used in all conditions tested.

Extended-exposure condition. The complete trajectory of the green bar was visible. The bar's intensity was set at a value that produced a colour match of the lines in the brief-exposure condition. On ten trials the observer adjusted the intensity of the comparison line's green component to achieve a colour match between the lines.

Wide-bar and tracking conditions. A wide bar ($1.59° \times 2.0°$) was used to test the contribution of motion *per se* to the colour effect (see text). In the tracking condition, observers used smooth-pursuit eye movements to follow the bar of original size ($1.59° \times 0.20°$).

Persistence reduction through visual masking. Introduction of a visual mask in the brief exposure condition required an additional viewing channel which involved several changes in the optical arrangement. Consequently, the brief and extended exposure conditions were repeated. The mask consisted of two flanking bars, abutting the original bar with no gap or overlap, flashed for 10 ms. Each flanking bar was either $1.59° \times 0.20°$ or $1.59° \times 0.40°$. The intensity of the flanking bars was equated to that of the original bar by using modified 'minimally distinct border' technique[28].

Received 7 May 1996; accepted 9 January 1997.

1. Hurvich, L. M. & Jameson, D. The binocular fusion of yellow in relation to color theories. *Science* **114,** 199–202 (1951).
2. Hecht, S. On the binocular fusion of colors and its relation to theories of color vision. *Proc. Natl Acad. Sci. USA* **14,** 237–241 (1928).
3. Zeki, S. M. The functional organization of projections from striate to prestriate visual cortex in the rhesus monkey. *Cold Spring Harb. Symp. Quant. Biol.* **40,** 591–600 (1975).
4. Livingstone, M. S. & Hubel, D. H. Psychophysical evidence for separate channels for the perception of form, color, movement, and depth. *J. Neurosci.* **7,** 3416–3468 (1987).
5. Ramachandran, V. S. & Gregory, R. L. Does colour provide an input to human motion perception? *Nature* **275,** 55–56 (1978).
6. Cavanagh, P., Tyler, C. W. & Favreau, O. E. Perceived velocity of moving chromatic gratings. *J. Opt. Soc. Am.* **1,** 893–899 (1984).
7. Saito, H., Tanaka, K., Isono, H., Yasuda, M. & Mikami, A. Directionally selective response of cells in the middle temporal area (MT) of the macaque monkey to the movement of equiluminous opponent color stimuli. *Exp. Brain Res.* **75,** 1–14 (1989).
8. Cropper, S. J. & Derrington, A. M. Rapid colour-specific detection of motion in human vision. *Nature* **379,** 72–74 (1996).
9. MacKay, D. M. Perceptual stability of a stroboscopically lit visual field containing self-luminous objects. *Nature* **181,** 507–508 (1958).
10. Nijhawan, R. Motion extrapolation in catching. *Nature* **370,** 256–257 (1994).
11. Hurvich, L. M. *Color Vision* (Sinauer, Sunderland, Massachusetts, 1981).
12. Walraven, J. Spatial characteristics of chromatic induction; the segregatin of lateral effects from straylight artefacts. *Vision Res.* **13,** 1739–1753 (1973).
13. Khurana, B. & Nijhawan, R. Extrapolation or attention shift? *Nature* **378,** 565–566 (1995).
14. Aho, A.-C., Donner, K., Helenius, S., Olesen Larsen, L. & Reuter, T. Visual performance of the toad (*Bufo bufo*) at low light levels: retinal ganglion cell responses and prey-catching accuracy. *J. Comp. Physiol.* **172,** 671–682 (1993).
15. Richards, W. Visual suppression during passive eye movement. *J. Opt. Soc. Am.* **58,** 1159–1160 (1968).
16. Land, E. H. & McCann, J. J. Lightness and the retinex theory. *J. Opt. Soc. Am.* **61,** 1–11 (1971).
17. Gilchrist, A. The perception of surface blacks and whites. *Sci. Am.* **24,** 88–97 (1979).
18. Efron, R. The minimum duration of a perception. *Neuropsychologia* **8,** 57–63 (1970).
19. Hogben, J. H. & Di Lollo, V. Perceptual integration and perceptual segregation of brief visual stimuli. *Vision Res.* **14,** 1059–1069 (1974).
20. Burr, D. Motion smear. *Nature* **284,** 164–165 (1980).
21. Morgan, M. J. Perception of continuity in stroboscopic motion: A temporal frequency analysis. *Vision Res.* **19,** 491–500 (1979).
22. Kahneman, D. Method, findings, and theory in studies of visual masking. *Psychol. Bull.* **70,** 404–425 (1968).
23. Alpern, M. & Rushton, W. A. H. The specificity of the cone interaction in the after-flash effect. *J. Physiol.* **176,** 473–482 (1965).
24. Yellott, J. I. & Wandell, B. A. Color properties of the contrast flash effect: Monoptic vs dichoptic comparisons. *Vision Res.* **16,** 1275–1280 (1976).
25. Di Lollo, V. & Hogben, J. H. Suppression of visible persistence as a function of spatial separation between inducing stimuli. *Percept. Psychophys.* **41,** 345–354 (1987).
26. Hubel, D. H. & Wiesel, T. N. Receptive fields and functional architecture of monkey striate cortex. *J. Physiol. (Lond.)* **195,** 215–243 (1968).
27. Duhamel, J.-R., Colby, C. L. & Goldberg, M. E. The updating of the representation of visual space in parietal cortex by intended eye movements. *Science* **255,** 90–92 (1992).
28. Boynton, R. M. in *Visual Psychophysics and Physiology* (eds Armington, J. C., Krauskopf, J. & Wooten, B. R.) 193–207 (Academic, New York, 1978).
29. Zeki, S. The representation of colours in the cerebral cortex. *Nature* **284,** 412–418 (1980).

Acknowledgements. This work would not have been possible without the constant interest and support of B. Khurana. I thank P. Cavanagh for his contributions; K. Nakayama for the use of the Vision Sciences Laboratory, Harvard University; T. Reuter and the A. Treisman group for their interest; A. Derrington, R. Singh, I. Thornton, A. Gilchrist, J. Cutting, M. Morgan and O. Braddick for comments and discussion; and E. Snyder and F. Horan for technical assistance.

Correspondence and requests for materials should be addressed to the author (e-mail: rn15@cornell.edu).

Adaptation of retinal processing to image contrast and spatial scale

Stelios M. Smirnakis*†, Michael J. Berry‡, David K. Warland‡, William Bialek§ & Markus Meister‡

*Departments of * Physics, and ‡ Molecular and Cellular Biology, Harvard University, 16 Divinity Avenue, Cambridge, Massachusetts 02138, USA*
† Division of Health Sciences and Technology, Harvard Medical School, 260 Longwood Avenue, Boston, Massachusetts 02115, USA
§ NEC Research Institute, Princeton, New Jersey 08540, USA

Owing to the limited dynamic range of a neuron's output, neural circuits are faced with a trade-off between encoding the full range of their inputs and resolving gradations among those inputs. For example, the ambient light level varies daily over more than nine orders of magnitude[1], whereas the firing rate of optic nerve fibres spans less than two[2]. This discrepancy is alleviated by light adaptation[3]: as the mean intensity increases, the retina becomes proportionately less sensitive. However, image statistics other than the mean intensity also vary drastically during routine visual processing. Theory predicts that an efficient visual encoder should adapt its strategy not only to the mean, but to the full shape of the intensity distribution[4–6]. Here we report that retinal ganglion cells, the output neurons of the retina, adapt to both image contrast—the range of light intensities—and to spatial correlations within the scene, even at constant mean intensity. The adaptation occurs on a scale of seconds, one hundred times

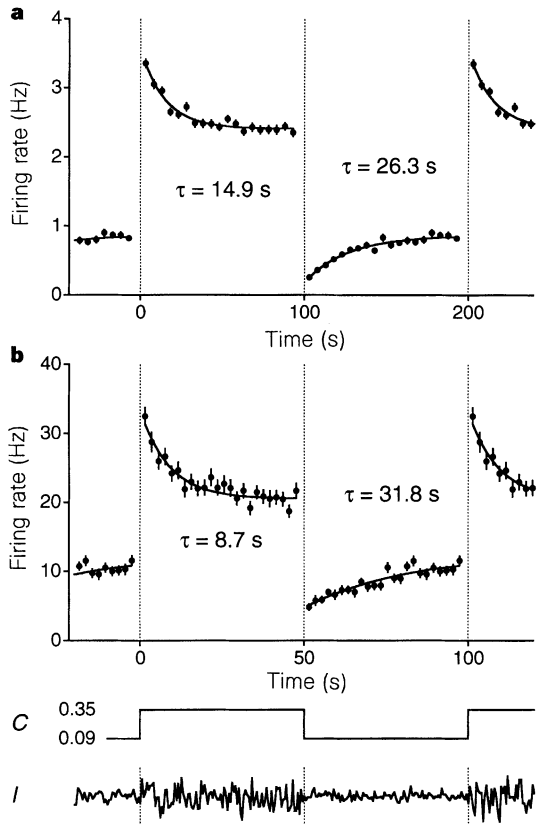

Figure 1 Firing rate of a salamander (**a**) and a rabbit (**b**) ganglion cell under spatially uniform flicker stimulation, alternating every 100 (**a**) or 50 (**b**) seconds between contrast values of 0.09 and 0.35. Average firing rate values were computed in 5-s (**a**) or 2-s (**b**) time bins over 100 (**a**) or 25 trials (**b**). Continuous lines are exponential fits with decay time τ. The first and last segments are periodic repeats of the data. Trace below (**b**) shows the time course of the contrast, C. Bottom trace illustrates the time course of the flickering intensity, I; note that the random flicker sequence was different in each stimulus trial. Similar gradual changes in the firing rate were unambiguous in 75% of salamander and 51% of rabbit cells. Another 18% in salamander and 31% in rabbit showed the gradual firing rate decline after a contrast increase but no detectable recovery following a contrast decrease.

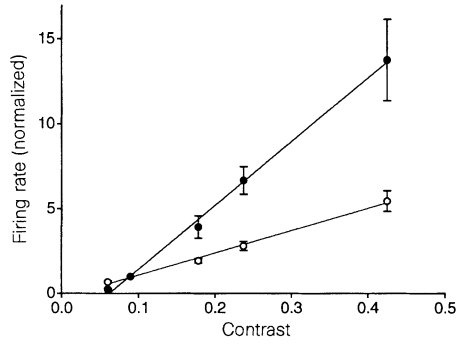

Figure 2 Initial firing rate (R_i, closed symbols) and final firing rate (R_f, open symbols) following a contrast step from $C = 0.09$ to values ranging between 0.06 and 0.43. For each cell, R_i and R_f were calculated as in Table 1 and normalized to yield $R_i = 1$ at $C = 0.09$, then averaged over 53 salamander ganglion cells from 2 retinae. Lines are linear fits.

more slowly than the immediate light response, and involves 2–5-fold changes in the firing rate. It is mediated within the retinal network: two independent sites of modulation after the photoreceptor cells appear to be involved. Our results demonstrate a remarkable plasticity in retinal processing that may contribute to the contrast adaptation of human vision[7].

We recorded the spike trains of ganglion cells in the isolated retina of a tiger salamander or rabbit. The photoreceptor layer was presented with random flicker stimuli whose mean intensity remained constant throughout, but whose second-order statistics changed abruptly at long intervals (see Methods). The goal was to monitor changes in retinal processing that are brought about by such a switch in the properties of the artificial visual environment. The first set of experiments employed a spatially uniform flickering field; its mean intensity was kept constant, but the width of the intensity distribution increased or decreased abruptly. Following such a step increase in contrast, the firing rate of most retinal ganglion cells increased abruptly, then decayed exponentially to a much lower value (Fig. 1 and Table 1). Following the opposite contrast step, the firing rate dropped abruptly and then recovered exponentially. These gradual changes in the firing rate suggest an adaptive modification of ganglion cell response properties following a step in contrast. For most salamander cells, the decay of the firing rate after a contrast increase was 2 to 3 times faster than its recovery following a contrast decrease (Table 1). Rabbit ganglion cells adapted very similarly (Fig. 1b and Table 1), even though their absolute firing rates were an order of magnitude higher than those of salamander ganglion cells. 'On' and 'off' cells showed no qualitative differences in their adaptation behaviour to this stimulus.

The initial firing rate immediately following a contrast jump

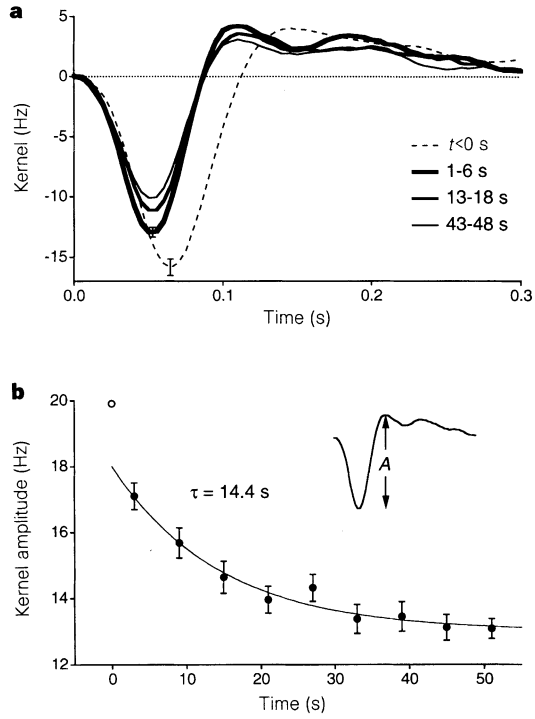

Figure 3 a, The effect of a contrast step from $C = 0.09$ to 0.35 on the linear kernel of a salamander ganglion cell (from Fig. 1a): just before the step (broken line), after the step at 1–6 s (thick line), 13–18 s (medium line), and 43–48 s (thin line). The kernel $k(t)$ was computed with 5-ms bins over the respective time interval and averaged over 50 stimulus trials (see Methods). **b**, Peak-to-peak amplitude (inset) of the kernel from the cell in (**a**), as a function of time relative to the contrast transition. Open symbol represents value at $t < 0$. Continuous line is an exponential fit to data after the step, with decay time τ. A similar decrease of the kernel amplitude was observed in 93% of salamander and 85% of rabbit cells.

increased linearly with the final contrast (Fig. 2). The steady-state firing rate, after the exponential transient, also varied linearly with the contrast. However, the latter curve was less than half as steep as the former, a clear sign of contrast adaptation. Using the same criterion, but different stimuli, a small but significant contrast adaptation effect has been demonstrated in the cat's lateral geniculate nucleus[8].

To determine how each ganglion cell responded to the flickering light, we computed the linear kernel of its firing rate with respect to the stimulus intensity[9,10]; this can also be viewed as the linear response to a brief flash of light (see Methods). A step increase in contrast triggered a rapid change in the shape of this kernel towards a faster waveform (Fig. 3a, broken and thick lines). This was followed by a gradual decrease of the kernel amplitude (Fig. 3 and Table 1). Following the opposite contrast step, the kernel shape reverted and its amplitude gradually increased. The fact that the slow changes in kernel amplitude and firing rate occur with a very similar time course (Figs 1a and 3b) suggests that the rate modulations truly reflect a change in the sensitivity of the light response. At low contrast, a high sensitivity serves to represent effectively the narrow range of intensities. Following a sudden transition to high contrast, the sensitivity gradually decreases to encode the broader intensity range.

Previous studies of retinal signalling in cat[11] and catfish[9] indicated that ganglion cell response properties change as a function of ambient contrast. This 'contrast gain control' occurred within tens of milliseconds[12] of a contrast step, which is less than the photoreceptor integration time. Figure 3a also shows a shift of ganglion cell sensitivity towards higher temporal frequencies that occurs immediately after the contrast step, as seen in cat[11]. These fast changes can be viewed as a nonlinear feature of the instantaneous light response[13], rather than as gradual adaptation to scene statistics. By comparison, the subsequent adaptation phase documented here requires seconds to tens of seconds. This is similar to the time in which an animal might move into an environment of substantially different texture, or in which the scene illumination might change from direct to diffuse light, producing a change in contrast.

Some neural element within the retina must sense the contrast and control the change in sensitivity. To estimate the size of this neuron's receptive field, we stimulated the salamander retina alternatingly with a flickering checkerboard of varying square size, D, and spatially uniform flicker of the same mean and contrast (see Methods). Under these conditions, only neurons whose receptive field extended over more than one square of the checkerboard experienced a change in the statistics of their synaptic input as a result of the transition to uniform flicker.

Figure 4a illustrates the firing rate of a salamander ganglion cell in such an experiment. Following a transition from uniform to checkerboard stimulation, the firing rate suddenly increased, then gradually declined over several seconds to a steady state. Following the reverse transition, the firing rate suddenly decreased, then gradually recovered. Judging from the final steady-state firing rate, the neuron was driven more strongly by checkerboards than by uniform fields, consistent with the centre-surround antagonism in its receptive field. During the adaptation phase, the neuron's sensitivity always declined when exposed to a stronger stimulus, and recovered under a weaker stimulus, analogous to the observations with uniform stimulation at varying contrast (Fig. 1). Thus, the same mechanism may account for both observations (Fig. 5). Such behaviour was seen in all 'on' cells.

However, the great majority of 'off' ganglion cells behaved like the neuron shown in Fig. 4b. During the adaptation phase the neuron's

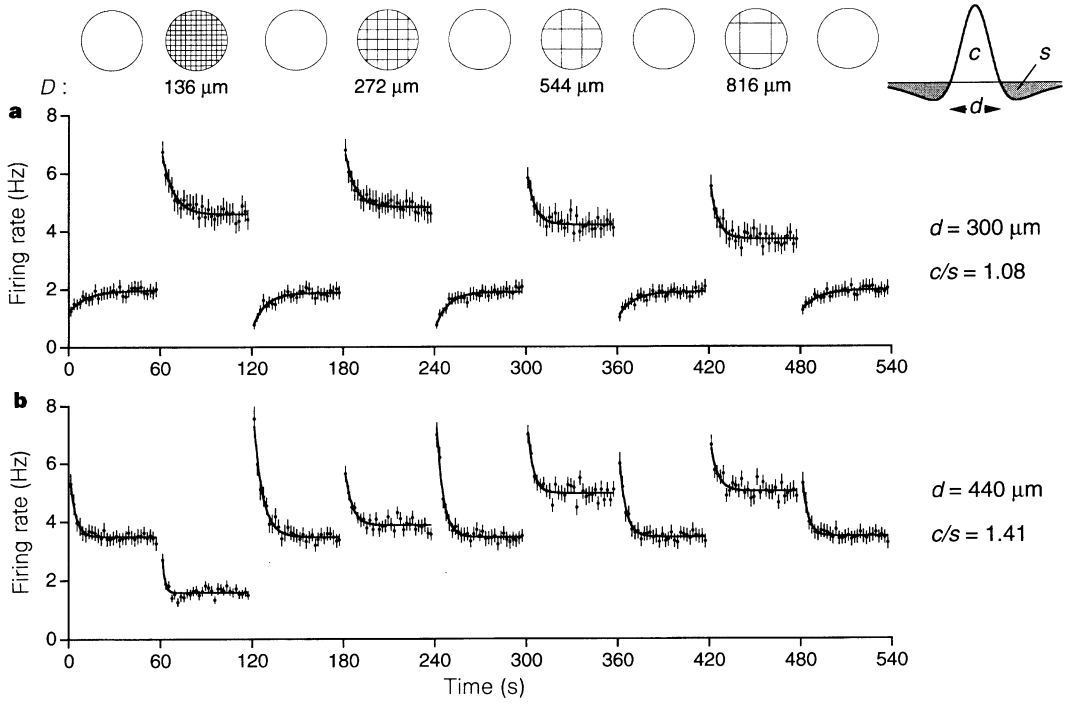

Figure 4 Adaptation to a change in spatial scale for two salamander ganglion cells, 'on' type (**a**) and 'off' type (**b**). Top row illustrates time course of the stimulus during a trial, alternating between uniform and checkerboard stimulation at varying square size, D. The checkerboard was also shifted every 30 ms by a spatial offset chosen at random on a 136-μm grid; this ensured that checker boundaries would not consistently fall on the same neural receptive fields. Contrast remained at $C = 0.24$ throughout. Average firing rates were computed in 2-s intervals over 50 trials. Lines are exponential fits. The last data segment (480–540 s) is identical to the first (0–60 s). The receptive field profiles (see Methods) of both cells are summarized (right) by the diameter of the centre region, d, and the ratio of integrated sensitivity in the positive centre to that in the negative surround, c/s. Note that the steady-state firing rates are maximal when $D \approx d$, and are suppressed more under uniform illumination when the surround is stronger, as in **a**. 12% of recorded neurons showed adaptation as in **a**, 82% as in **b**; for 6% the firing rate adapted downwards only following the transition from uniform to checkerboard stimulation. In the rabbit retina these stimuli produced qualitatively similar adaptation of the ganglion cell firing rate, but there was no sharp distinction between 'on' and 'off' cells.

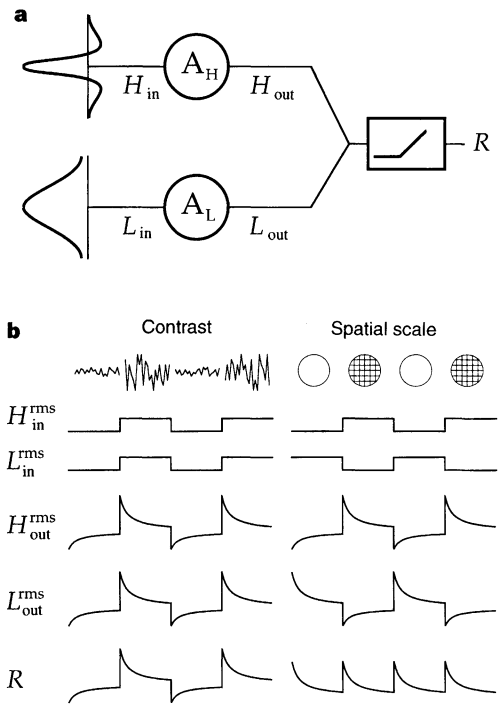

Figure 5 a, Model of contrast adaptation. Two pathways lead from the stimulus to the ganglion cell: one (H, 'high pass') integrates the stimulus with a spatially antagonistic receptive field; the other (L, 'low pass') has a broad receptive field. Each pathway contains an adaptive neuron (A_H, A_L) which gradually increases its sensitivity when its input signal (H_{in}, L_{in}) varies over a small range, and gradually decreases its sensitivity when its input range is large. The output signals of the two pathways (H_{out}, L_{out}) are pooled and rectified to produce a positive ganglion cell firing rate (R). **b**, Predictions for the firing rate under variations in contrast (left) or checkerboard-square size (right). The range of signals in the H and the L pathways are indicated by their root-mean-square variations, H^{rms} and L^{rms}. When the flicker contrast is stepped up (left), both pathways are driven more strongly and thus adapt by decreasing their sensitivity, resulting in a gradual decline in the firing rate. The opposite is predicted when the contrast steps down. When switching from uniform to checkerboard stimulation (right), the H pathway is driven more strongly and the L pathway more weakly. Thus their sensitivities adapt in the opposite direction. As the downward adaptation transients are larger than the upward transients (Fig. 1), the net effect is a gradual decline of the firing rate. When switching back to uniform stimulation, the roles of H and L pathways are switched, but their pooled activity again results in a gradual decline of the firing rate. This can explain the behaviour of salamander 'off' cells in Fig. 1a (left) and Fig. 4b (right). 'On' cells behave as though they lack the L pathway, or at least its adaptive control, because their firing rate under both conditions (Figs 1a and 4a) varies as the output signal in the H pathway.

Table 1 Characteristics of adaptation transients induced by changes in contrast

	Contrast		τ(s)		R_i/R_f		A_i/A_f	
	C_{low}	C_{high}	↑	↓	↑	↓	↑	↓
Salamander	0.06	0.18	9.1 ± 0.9 (44)	17.8 ± 1.7 (24)	2.48 ± 0.31 (44)	0.18 ± 0.04 (24)	1.48 ± 0.07 (42)	0.56 ± 0.06 (17)
	0.09	0.35	8.8 ± 1.1 (20)	28.5 ± 2.7 (17)	1.69 ± 0.14 (20)	0.37 ± 0.06 (17)	1.26 ± 0.05 (20)	0.60 ± 0.07 (16)
Rabbit	0.09	0.35	12.6 ± 1.28 (36)	27.3 ± 2.7 (16)	2.26 ± 0.27 (36)	0.27 ± 0.06 (16)	1.45 ± 0.13 (29)	0.68 ± 0.07 (16)

Changes in contrast from C_{low} to C_{high} are indicated by an upward arrow, and from C_{high} to C_{low} by a downward arrow. For each cell, the time course of the firing rate was fitted with an exponential of time constant τ (Fig. 1) and extrapolated to yield the initial and final firing rate, R_i and R_f. The kernel amplitude, A, was taken as the peak-to-peak amplitude of the waveform (Fig. 3b), and its initial and final values, A_i and A_f, were measured over the first and the last 5-s interval of the contrast segment respectively. The parameters τ, R_i/R_f, and A_i/A_f were averaged over all cells that showed adaptation (Figs 1 and 3), except when τ or A could not be determined accurately. The number of cells for each estimate is given in parentheses. Uncertainties denote standard error.

sensitivity was initially high and gradually declined following every stimulus transition, irrespective of whether the final rate increased or decreased. In fact, the final rate under 272-μm squares was almost identical to that under uniform stimulation, yet the transition produced a large transient during which the rate changed by more than a factor of two. This behaviour cannot be explained by a single mechanism of local contrast adaptation, but could result from independent adaptation in two pathways, one of which responds best at high spatial frequencies, the other at low frequencies (Fig. 5).

In these experiments, both the mean and the local contrast were held constant, and the adaptation process was triggered purely by a change in the spatial scale of the scene. These results place strong constraints on the site of adaptation. In particular, it does not occur in photoreceptors: The receptive field of cones—including their electrical coupling which extends over ~25 μm in turtle[14]—is too small to detect the difference between checkerboard and uniform stimulation. In the scheme proposed in Fig. 5, the H pathway must have a narrow centre, with a large surround extending over more than 800 μm (the largest square size tested). Bipolar cells—with their broad antagonistic surrounds from the horizontal cell syncitium[15,16]—could serve this role, as could the ganglion cell itself. The L pathway could be implemented by wide-field amacrine cells in the inner retina[17,18]. These assignments and the scheme in Fig. 5 are tentative, but they provide one framework for explaining the contrast adaptation behaviour of ganglion cells.

The effects reported here share several characteristics with contrast adaptation observed in human subjects and in the responses of cortical neurons. After adapting to a drifting grating, the threshold for detecting a similar test grating is raised about 5-fold[7], comparable in magnitude to the observed changes in the firing rate of retinal ganglion cells (Table 1, and see ref. 19). The time constants of psychophysical contrast adaptation also range from second to tens of seconds[7,20]. The loss of sensitivity after a contrast increase and the recovery after a contrast decrease often follow a different time course[21–23], a consistent feature in our recordings (Fig. 1 and Table 1; $P < 0.001$). Although this suggests that retinal processing is important in psychophysical contrast adaptation, cortical mechanisms certainly contribute as well, because there is partial interocular transfer of adaptation[7,20,24] and neurons in the cat visual cortex adapt more strongly to grating stimuli than neurons in the lateral geniculate nucleus[8].

In summary, it appears that visual processing in the retina is considerably more adaptive than previously acknowledged and adjusts not only to the mean illumination but also to both the range of intensity fluctuations and their spatial scale. Essentially identical behaviour was observed in a mammalian and an amphibian species, and related effects are seen in an insect visual system[5], suggesting that this strategy is a general principle of retinal processing. More broadly, it might be expected that any neural circuit would benefit from an adaptive control that responds to changes in the statistics of its inputs. The retina, with its accessible and well studied circuitry, is ideal for studying the underlying mechanisms. □

Methods

Recording. Retinae of larval tiger salamanders and Dutch belted rabbits were isolated in darkness into oxygenated Ringer's medium[10] (salamander) or Ames'

solution (rabbit; Sigma A-1420 supplemented with 22.6 mM Na_2HCO_3, 4.4 mM D-glucose, pH 7.4; maintained at 37 °C during recording). A piece of retina 2–4 mm on a side was placed onto a flat multi-electrode array for extracellular recording from the ganglion cell layer[10,25]. Results are reported from 71 cells in 4 salamander retinae, 55 cells in 2 rabbit retinae (Figs 1, 2, 3; Table 1), and 33 cells in 2 salamander retinae (Fig. 4). In the salamander, 14% of recorded ganglion cells were 'on' and 86% 'off'. In the rabbit, 33% were 'on', 51% 'off', and 16% had mixed response properties.

Stimulation. Stimuli were projected from a computer monitor onto a 3.25-mm-diameter aperture on the retina. Patterns consisted of a single uniform field of flickering light (Figs 1–3) or a flickering checkerboard with independently modulated square fields (Fig. 4), ranging in size, D, from 0.068 to 0.816 mm. The light intensity of each field was chosen every $\Delta t = 30$ ms at random from a gaussian probability distribution with mean M and standard deviation W. Contrast, C, was defined as W/M. The field size D sets the spatial scale of the stimulus. All experiments used white light[26] with a mean intensity of $M = 4.2\,\mathrm{mW\,m^{-2}}$ at the retina. The equivalent photon flux at the peak absorption wavelength (λ_{max}) was 5,680 photons $\mu m^{-2}\,s^{-1}$ for the salamander's red cone photoreceptor ($\lambda_{max} = 630$ nm), and 5,150 photons $\mu m^{-2}\,s^{-1}$ for the rabbit's green cone ($\lambda_{max} = 523$ nm)[27,28].

Analysis. In a typical experiment, we interleaved segments of two stimulus types in the order $A_1B_1A_2B_2A_3B_3...$, where the A_i represents segments with the same contrast and spatial scale, but different random flicker sequences, and B_i represent segments with another contrast or spatial scale. Individual segments of A and B lasted either 50 s or 100 s, and recordings extended over 25 to 100 AB trials. The mean firing rate at a given time around the A-to-B transition (Figs 1, 2, 4) was computed by counting the spikes in the corresponding short time bin of all the AB trials, and dividing by the number of trials and the length of the time bin. The first-order Wiener kernel (Fig. 3) of the response was computed by correlating the stimulus intensity $I(t)$ and the firing rate $R(t)$: $k(t) = \frac{1}{WC}\frac{1}{T}\int_0^T (I(t') - M)R(t' + t)\mathrm{d}t'$. This represents the linear effect on the firing rate from a flash of light with integrated intensity $M{\cdot}\Delta t$. The kernel at a given time around the transition was computed by performing the integral only over the corresponding time bins of all individual trials. The spatial receptive field (Fig. 4) was determined from steady-state responses to checkerboard stimulation with 136-μm squares: the kernel $k(t)$ was computed for each square, and its peak amplitude plotted as a function of position. All error bars in figures represent the standard error across trials.

Received 10 September 1996; accepted 9 January 1997.

1. Rushton, W. A. Visual Adaptation (The Ferrier Lecture, 1962). *Proc. R. Soc. Lond. B* **162,** 20–46 (1965).
2. Barlow, H. B. Critical limiting factors in the design of the eye and visual cortex (The Ferrier Lecture, 1980). *Proc. R. Soc. Lond. B* **212,** 1–34 (1981).
3. Shapley, R. & Enroth-Cugell, C. Visual Adaptation and Retinal Gain Controls. *Progr. Ret. Res.* **3,** 263–346 (1984).
4. Laughlin, S. A simple coding procedure enhances a neuron's information capacity. *Z. Naturforsch.* **36,** 910–912 (1981).
5. de Ruyter van Steveninck, R. R., Bialek, W., Potters, M. & Carlson, R. H. Statistical adaptation and optimal estimation in movement computation by the blowfly visual system. *Proc. IEEE Int. Conf. Systems, Man, and Cybernetics* 302–308 (1994).
6. DeWeese, M. & Bialek, W. Information flow in sensory neurons. *Il Nuovo Cimento* **17D,** 733–738 (1995).
7. Blakemore, C. & Campbell, F. W. On the existence of neurones in the human visual system selectively sensitive to the orientation and size of retinal images. *J. Physiol.* **203,** 237–260 (1969).
8. Ohzawa, I., Sclar, G. & Freeman, R. D. Contrast gain control in the cat's visual system. *J. Neurophysiol.* **54,** 651–667 (1985).
9. Sakai, H. M. & Naka, K. Signal transmission in the catfish retina. V. Sensitivity and circuit. *J. Neurophysiol.* **58,** 1329–1350 (1987).
10. Meister, M., Pine, J. & Baylor, D. A. Multi-neuronal signals from the retina: acquisition and analysis. *J. Neurosci. Meth.* **51,** 95–106 (1994).
11. Shapley, R. M. & Victor, J. D. The effect of contrast on the transfer properties of cat retinal ganglion cells. *J. Physiol.* **285,** 275–298 (1978).
12. Victor, J. D. The dynamics of the cat retinal X cell centre. *J. Physiol.* **386,** 219–246 (1987).
13. Wang, J.-L. & Naka, K.-I. Contrast gain control in the lower vertebrates retinas. *Soc. Neurosci. Abstr.* **21,** 1644 (1995).
14. Copenhagen, D. R. & Green, D. G. The absence of spread of adaptation between rod photoreceptors in turtle retina. *J. Physiol.* **369,** 161–181 (1985).
15. Dacheux, R. F. & Raviola, E. Horizontal cells in the retina of the rabbit. *J. Neurosci.* **2,** 1486–1493 (1982).
16. Hare, W. A. & Owen, W. G. Spatial organization of the bipolar cell's receptive field in the retina of the tiger salamander. *J. Physiol.* **421,** 223–245 (1990).
17. Werblin, F., Maguire, G., Lukasiewicz, P., Eliasof, S. & Wu, S. M. Neural interactions mediating the detection of motion in the retina of the tiger salamander. *Visual Neurosci.* **1,** 317–329 (1988).
18. Bloomfield, S. A. Relationship between receptive and dendritic field size of amacrine cells in the rabbit retina. *J. Neurophysiol.* **68,** 711–725 (1992).
19. Barlow, H. B. & Hill, R. M. Evidence for a physiological explanation of the waterfall phenomenon and figural after-effects. *Nature* **200,** 1345–1347 (1963).
20. Schieting, S. & Spillmann, L. Flicker adaptation in the peripheral retina. *Vision Res.* **27,** 277–284 (1987).
21. Albrecht, D. G., Farrar, S. B. & Hamilton, D. B. Spatial cntrast adaptation characteristics of neurones recorded in the cat's visual cortex. *J. Physiol.* **347,** 713–739 (1984).
22. Ho, W. A. & Berkley, M. A. Evoked potential estimates of the time course of adaptation and recovery to counterphase gratings. *Vision Res.* **28,** 1287–1296 (1988).
23. Giaschi, D., Douglas, R., Marlin, S. & Cynader, M. The time course of direction-selective adaptation in simple and complex cells in cat striate cortex. *J. Neurophysiol.* **70,** 2024–2034 (1993).
24. Barlow, H. B. & Bridley, G. S. Inter-ocular transfer of movement aftereffects during pressure binding of the stimulated eye. *Nature* **200,** 1347 (1963).
25. Meister, M., Lagnado, L. & Baylor, D. A. Concerted signaling by retinal ganglion cells. *Science* **270,** 1207–1210 (1995).
26. Brainard, D. Calibration of a computer controlled color monitor. *Color Res. Appl.* **14,** 23–34 (1989).
27. Dawis, S. M. Polynomial expressions of pigment nomograms. *Vision Res.* **21,** 1427–1430 (1981).
28. Nuboer, J. F. W. & Moed, P. J. Increment-threshold spectral sensitivity in the rabbit. *J. Comp. Physiol.* **151,** 353–358 (1983).

Acknowledgements. We thank T. Jordan for help with rabbit experiments, the members of our group and B. Chang for discussion, and D. Baylor, J. Dowling, C. Reid, F. Rieke and J. Victor for comments on the manuscript. Supported by a grant from the Office of Naval Research and a Markey Scholarship to M.M., and a Research Assistantship from the Harvard–MIT Division of Health Sciences and Technology to S.S.

Correspondence and requests for materials should be addressed to M.M. (e-mail: meister@biosun.harvard.edu).

An endothelial receptor for oxidized low-density lipoprotein

Tatsuya Sawamura*, Noriaki Kume†, Takuma Aoyama*, Hideaki Moriwaki†, Hajime Hoshikawa*, Yuichi Aiba‡, Takeshi Tanaka§, Soichi Miwa*, Yoshimoto Katsura‡, Toru Kita† & Tomoh Masaki*

** Department of Pharmacology and † Department of Geriatric Medicine, Faculty of Medicine, Kyoto University, Kyoto 606, Japan*
‡ Department of Immunology, Chest Disease Research Institute, Kyoto University, Kyoto 606, Japan
§ Japan Red Cross Saitama Branch, Yono, Saitama 338, Japan

Endothelial dysfunction or activation elicited by oxidatively modified low-density lipoprotein (Ox-LDL) has been implicated in the pathogenesis of atherosclerosis[1–4], characterized by intimal thickening and lipid deposition in the arteries. Ox-LDL and its lipid constituents impair endothelial production of nitric oxide, and induce the endothelial expression of leukocyte adhesion molecules and smooth-muscle growth factors, which may be involved in atherogenesis[5–7]. Vascular endothelial cells in culture[8,9] and *in vivo*[10,11] internalize and degrade Ox-LDL through a putative receptor-mediated pathway that does not involve macrophage scavenger receptors[12–15]. Here we report the molecular cloning, using expression cloning strategy, of an Ox-LDL receptor from vascular endothelial cells. The cloned receptor is a membrane protein that belongs structurally to the C-type lectin family, and is expressed *in vivo* in vascular endothelium and vascular-rich organs.

A cDNA library of cultured bovine aortic endothelial cells (BAEC), which bind, internalize and degrade Ox-LDL, was used for expression cloning. COS-7 cells transfected with a single clone, pBLOX-1, exhibited prominent uptake of DiI-labelled Ox-LDL. To characterize the protein encoded by pBLOX-1, designated lectin-like Ox-LDL receptor (LOX-1), as a receptor for Ox-LDL, we have transfected pBLOX-1 into CHO-K1 cells and established a cell line stably expressing bovine LOX-1 (BLOX-1-CHO). An antiserum was also developed using bacterially expressed extracellular domain of LOX-1(61–270) as an antigen. Immunoblotting of total cell lysate of BLOX-1-CHO, using anti-LOX-1 antiserum, showed a single band with approximate relative molecular mass 50,000 (M_r 50K). This particular band was not detected in cell lysate from untransfected CHO-K1 cells (Fig. 1a). A band with 50K on the same position of the